Clinical and Translational Report

Cell Stem Cell

CRISPR-Based Adenine Editors Correct Nonsense Mutations in a Cystic Fibrosis Organoid Biobank

Graphical Abstract

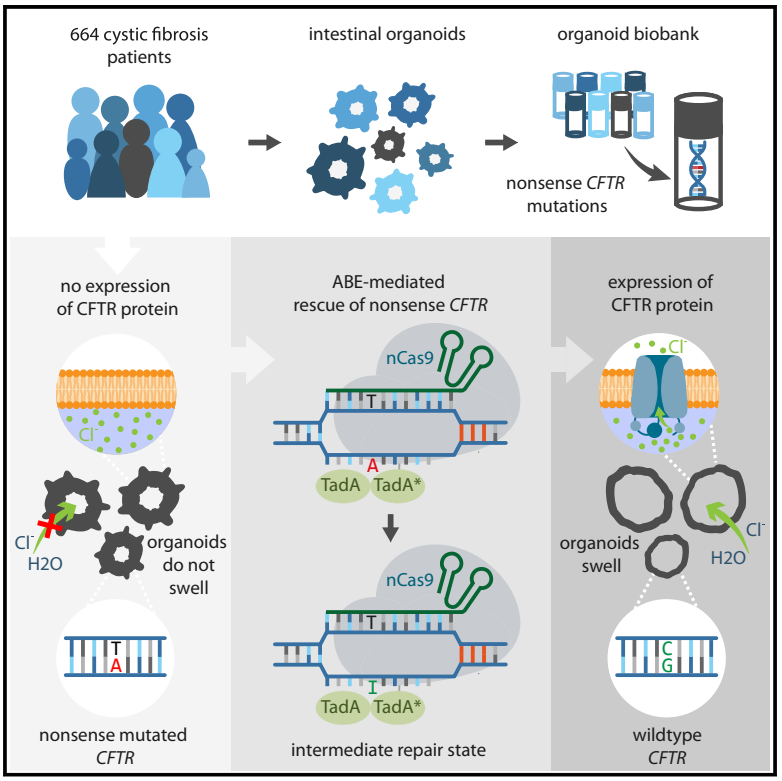

Highlights

- 664 patients and 154 *CFTR* mutations represented in an organoid biobank
- Adenine base editors enable efficient repair of nonsense mutations in *CFTR*
- xCas9 increases the target scope of *CFTR* repair in our biobank
- Adenine base editors cause no detectable off-target effects during repair

Authors

Maarten H. Geurts, Eyleen de Poel, Gimano D. Amatngalim, ..., Cornelis K. van der Ent, Jeffrey M. Beekman, Hans Clevers

Correspondence

j.beekman@umcutrecht.nl (J.M.B.), h.clevers@hubrecht.eu (H.C.)

In Brief

Here, we show the generation of an extensive cystic fibrosis patient-derived intestinal organoid biobank. We use this biobank to study gene correction by adenine base editors and show genetic repair of four selected nonsense mutations in *CFTR* without any genome-wide off-target effects on canonical and non-canonical PAMs.

Geurts et al., 2020, Cell Stem Cell *26*, 503–510
April 2, 2020
https://doi.org/10.1016/j.stem.2020.01.019

CellPress

Cell Stem Cell
Clinical and Translational Report

CRISPR-Based Adenine Editors Correct Nonsense Mutations in a Cystic Fibrosis Organoid Biobank

Maarten H. Geurts,[1,2,11] Eyleen de Poel,[3,4,11] Gimano D. Amatngalim,[3,4] Rurika Oka,[5,6] Fleur M. Meijers,[3,4] Evelien Kruisselbrink,[3,4] Peter van Mourik,[3] Gitte Berkers,[3] Karin M. de Winter-de Groot,[3] Sabine Michel,[3] Danya Muilwijk,[3] Bente L. Aalbers,[3] Jasper Mullenders,[7] Sylvia F. Boj,[7] Sylvia W.F. Suen,[3,4] Jesse E. Brunsveld,[3,4] Hettie M. Janssens,[8] Marcus A. Mall,[9,10] Simon Y. Graeber,[9,10] Ruben van Boxtel,[5,6] Cornelis K. van der Ent,[3] Jeffrey M. Beekman,[3,4,12,*] and Hans Clevers[1,2,12,13,*]

[1]Hubrecht Institute, Royal Netherlands Academy of Arts and Sciences (KNAW) and University Medical Center Utrecht, 3584 CT Utrecht, the Netherlands
[2]Oncode Institute, Hubrecht Institute, 3584 CT Utrecht, the Netherlands
[3]Department of Pediatric Respiratory Medicine, Wilhelmina Children's Hospital, University Medical Center, Utrecht University, 3584 EA Utrecht, the Netherlands
[4]Regenerative Medicine Utrecht, University Medical Center, Utrecht University, 3584 CT Utrecht, the Netherlands
[5]Princess Maxima Center, 3584 CS Utrecht, the Netherlands
[6]Oncode Institute, Princess Maxima Center, 3584 CS Utrecht, the Netherlands
[7]Hubrecht Organoid Technology, 3584 CM, Utrecht, the Netherlands
[8]Department of Pediatrics, division of Respiratory Medicine and Allergology, ErasmusMC-Sophia Children's Hospital, University Hospital Rotterdam, 3015 GD Rotterdam, the Netherlands
[9]Department of Pediatric Pulmonology, Immunology and Critical Care Medicine, Charité-Universitätsmedizin Berlin, 13353 Berlin, Germany
[10]Berlin Institute of Health (BIH), 10178 Berlin, Germany
[11]These authors contributed equally
[12]These authors contributed equally
[13]Lead Contact
*Correspondence: j.beekman@umcutrecht.nl (J.M.B.), h.clevers@hubrecht.eu (H.C.)
https://doi.org/10.1016/j.stem.2020.01.019

SUMMARY

Adenine base editing (ABE) enables enzymatic conversion from A-T into G-C base pairs. ABE holds promise for clinical application, as it does not depend on the introduction of double-strand breaks, contrary to conventional CRISPR/Cas9-mediated genome engineering. Here, we describe a cystic fibrosis (CF) intestinal organoid biobank, representing 664 patients, of which ~20% can theoretically be repaired by ABE. We apply SpCas9-ABE (PAM recognition sequence: NGG) and xCas9-ABE (PAM recognition sequence: NGN) on four selected CF organoid samples. Genetic and functional repair was obtained in all four cases, while whole-genome sequencing (WGS) of corrected lines of two patients did not detect off-target mutations. These observations exemplify the value of large, patient-derived organoid biobanks representing hereditary disease and indicate that ABE may be safely applied in human cells.

INTRODUCTION

Cystic fibrosis (CF) is a life-shortening disease, caused by a wide variety of mutations in the CF transmembrane conductance regulator (*CFTR*) gene (Sosnay et al., 2013). Recently developed pharmacotherapies ("CFTR modulators") restore CFTR protein function with impressive efficacy, acting on the most common mutant CFTR protein (*CFTR*-F508del) and potentially on other mutant CFTR proteins that share conformational defects with F508del (Keating et al., 2018; Ramsey et al., 2011). These treatments require lifelong administration and are not effective in most people with rare *CFTR* mutations. Therefore, permanent restoration of endogenous CFTR function using gene-editing techniques remains a favorable option. In a previous study, we have shown that "classic" CRISPR/Cas9-mediated homology-dependent repair (HDR) can be used to restore the *CFTR*-F508del mutation in intestinal organoids (Sato et al., 2011; Schwank et al., 2013). Functional repair of CFTR was assessed using a forskolin-induced swelling (FIS) assay, which is impaired in CF organoids and correlates with clinical disease severity (de Winter-de Groot et al., 2018) and *in vivo* CFTR modulator response (Berkers et al., 2019; Dekkers et al., 2013, 2016). This assay facilitated the rapid selection of genetically repaired, clonal organoids by phenotypic screening upon addition of forskolin. However, CRISPR/Cas9-mediated HDR is inefficient and may introduce deleterious off-target double-stranded breaks, hampering potential clinical application (Cho et al., 2014; Fu et al., 2013; Kosicki et al., 2018; Pattanayak et al., 2013). Recently developed Cas9 fusion proteins, so-called base editors, circumvent these issues. Fusion of a cytidine deaminase to a partially inactive nickase Cas9 protein allows for efficient C-G to T-A base changes (C-T base editing, or CBE), while a fusion with an evolved TadA heterodimer performs

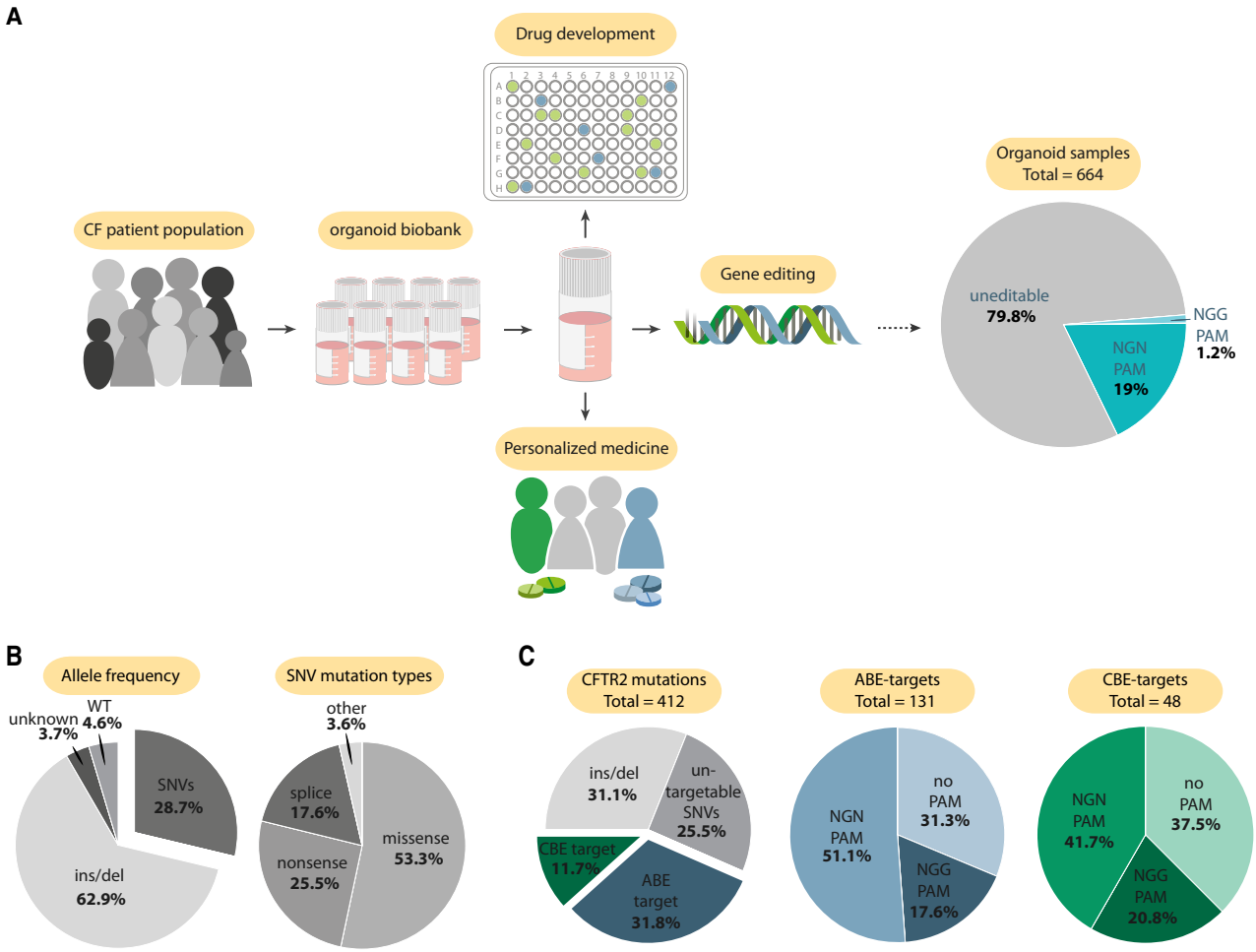

Figure 1. A CF Patient-Derived Intestinal Organoid Biobank

(A) Establishment and application of the CF patient-derived intestinal organoid biobank for drug development, personalized medicine, and gene editing. 20% of the organoid samples present in our biobank are eligible for base editing as these samples carry an editable mutation on at least one allele.

(B) Distribution of CFTR alleles and SNVs in our biobank.

(C) Frequency (%) of CFTR2 alleles targetable with single-base editing, where the blue fraction is ABE targetable and green fraction is CBE targetable, including a distribution of the CFTR2 alleles based on the presence of NGG and NGN PAMs.

See also Table S1.

the opposite reaction, from A-T to G-C (A-G base editing, or ABE) (Gaudelli et al., 2017; Koblan et al., 2018; Komor et al., 2016; Zafra et al., 2018). These DNA modulator proteins fused to Cas9 act on single-stranded DNA. Therefore, base editors act only within a small window of the single stranded R-loop that is generated upon Cas9 binding to the target sequence. This limited editing window, roughly base 4–8 within the protospacer, is defined by the specific localization of Cas9 proteins (Rees and Liu, 2018). Cas9 genomic localization is restricted by the protospacer adjacent motif (PAM) specificity of the protein, which is NGG for SpCas9 (Jinek et al., 2012; Mali et al., 2013). Recent developments have led to the generation of Cas9 alternatives such as xCas9 that show activity on the non-canonical PAM NGN, increasing the target range of base editing (Hu et al., 2018). Moreover, xCas9 has a higher fidelity than SpCas9 (and other Cas9 variants with less restrictive PAM requirements such as SpCas9-NG), making it a promising tool for genome engineering in a clinical setting (Nishimasu et al., 2018; Zhong et al., 2019).

RESULTS AND DISCUSSION

Generation of CF Patient-Derived Intestinal Organoid Biobank

To facilitate CF research, we generated and characterized an intestinal organoid biobank representing 664 CF patients, nearly half of the Dutch CF population (Figure 1A). Experimental controls within this biobank consist of 29 wild-type (WT) and 7 CF carrier samples (Tables S1A and S1B). This biobank covers the heterogeneity of CF mutations present in the Dutch CF population and the top 17 most prevalent mutations coincide with those in the Dutch CF registry (Figure 1B; Table S1C) (https://www.ncfs.nl/over-cystic-fibrosis/cf-registry-2017). Of note, as this biobanking effort has focused on infrequent CF alleles,

F508del/F508del homozygous organoids are underrepresented, while rare mutations are overrepresented. Indeed, we identified 61 rare mutations that are not present in the CFTR2 database (http://cftr2.org), currently the most comprehensive list of pathogenic mutations in *CF*. To our knowledge, 34 of these mutations have never been reported previously in CF patients (Tables S1D and S1E) (http://genet.sickkids.on.ca/).

We analyzed the number of mutations that are potentially targetable by base editing in the CFTR2 database (http://cftr2.org). Of all listed mutations in the CFTR2 database, 48 (11.7%) result from TA > CG conversions and can theoretically be repaired by CBEs. Of these mutations, 30 (62.5%) have a suitable PAM (10 for spCas9-CBE and an additional 20 for xCas9-CBE). In addition, 131 (31.8%) of the disease-causing mutations are caused by CG > TA conversions and can theoretically be rescued by ABEs, of which 90 (68.7%) have a suitable PAM (23 for spCas9-ABE, and an additional 67 for xCas9-ABE) (Figure 1C).

Functional Repair of CFTR using Adenine Base Editors on Canonical and Non-canonical PAMs

Next, we investigated base editing by SpCas9-ABE, which can theoretically correct *CFTR* mutations in 8 of the organoid samples in our biobank (1.2%) (Figure 1A). Four organoid samples harbored a mutation suitable for ABE as no additional adenines are present in the editing window or base editing of these residues would result in a synonymous base change. We chose to correct the R785X mutation, which is represented once as a homozygous mutation in our biobank. This mutation can be repaired by changing the adenine residue on position 5 of the protospacer sequence (Figures 2A and 2B). Editing of the single other adenine residue within the editing window would result in a synonymous mutation of the isoleucine residue on position 783 (I783I) (Figure 2B). We electroporated an estimated 1.5×10^6 single cells of this organoid line with the pCMV_ABEmax_P2A_GFP plasmid and single-guide RNA (sgRNA) plasmid. We observed hundreds of organoids that responded to forskolin as assessed by FIS, indicating the presence of corrected cells within each of these organoid lines (Figures S1A and S1D). Out of these FIS-assay-responsive organoids, three were randomly picked, and clonal lines were established by additional selection cycles, in which single cells were grown into single organoid structures that could be individually picked after visual screening for FIS (Figures S1A, S1D, and S1E). Next, Sanger sequencing was performed on the three generated clones to confirm clonal correction (Figure 2B). The repaired clonal organoid lines exhibited FIS at WT levels upon forskolin addition, whereas unrepaired clones did not display FIS (Figures 2C–2E). The SpCas9-ABE-mediated correction of *CFTR* was further confirmed by CFTR protein and mRNA analysis (Figure S2). We did observe editing of the 8th residue within the editing window in clone 2 (Figure 2B). As expected, this synonymous mutation did not result in altered FIS when compared to clones that did not carry this silent editing event (Figures 2C–2E). Editing efficiency of SpCas9-ABE (8.88%, n = 3) on this target mutation was 5-fold higher compared to conventional CRISPR/Cas9-mediated HDR with the use of single-stranded donor oligonucleotides (1.78%, n = 3) (Figures 2F and S3).

We next investigated base editing by xCas9-ABE, which has a more promiscuous PAM as compared to SpCas9-ABE. xCas9-ABE can theoretically correct 126 of the intestinal organoid samples in our biobank (19%), of which 50 lines do not have additional adenines in the editing window (Tables S2A and S2B). We first applied the technique on an organoid line homozygous for the most frequent nonsense mutation in our biobank, W1282X. This mutation can be repaired by converting the adenine on position 6 in the window (Figure 3A). Of note, editing on position 7 would result in a *de novo* R1283G mutation, never documented in CF patients and therefore possibly silent (http://genet.sickkids.on.ca/). Upon electroporation with the self-constructed pCMV_xABEmax_P2A_GFP plasmid and sgRNA plasmid, editing was observed only on the desired adenine at position 6 in the window, resulting in functional CFTR repair as shown by Sanger sequencing and FIS (Figures 3A, 3C, 3D, and 3F; Figures S1B and S1D). To investigate potential heterozygous ABE-mediated repair, we focused on the R553X mutation, the third most prevalent nonsense mutation as present in the CFTR2 database (http://cftr2.org). This mutation can be repaired by an A > G conversion at position 6 within the editing window, while no other adenines are present (Figure 3B). The selected organoid sample harbored a F508del mutation on the second allele. Again, genetic and functional repair of CFTR was observed upon electroporation with the self-constructed pCMV_xABEmax_P2A_GFP plasmid and sgRNA plasmid, as shown by Sanger sequencing and FIS (Figures 3B, 3C, 3D, and 3F; Figures S1B and S1D). The editing efficiencies of xCas9-ABE on the homozygous W1282X mutation (1.43%, n = 3) and the heterozygous R553X mutation were comparable (1.43%, n = 3) (Figure 3E; Figure S3). Hereby, we have shown that it is feasible to genetically correct both homozygous and heterozygous mutations in intestinal organoids using xCas9-ABE.

We confirmed the potential of xCas9-ABE in CF airway cells by growing nasal-brush-derived airway organoids from one patient, compound heterozygous for F508del, and the nonsense mutation R1162X. As airway organoid fluid secretion is not strictly CFTR dependent, FIS could not be utilized to detect functional repair (Sachs et al., 2019). We therefore electroporated the pCMV_xABEmax_P2A_GFP plasmid and the pertinent sgRNA plasmid together with a hygromycin piggyBac system to allow for selection of transfected organoids (Figure 3G). Sanger sequencing of 100 individually picked hygromycin-resistant clones revealed correct repair of the R1162X mutation in 8% of the organoids (Figure 3H).

No Detectable Off-Target Effects of Adenine Base Editors

To study potential off-target effects induced by each of the ABEs in homozygous and heterozygous repair, we performed whole-genome sequencing (WGS) analysis on three SpCas9-ABE (R785X/R785X) and three xCas9-ABE-repaired clones (R553X/F508del) and their respective unrepaired controls. Two recent studies in mouse and rice have shown that CBEs generate a high number of off-targets, while these are undetectable in ABE-treated samples (Jin et al., 2019; Zuo et al., 2019). To date, no genome-wide off-target studies have been performed in human cells to interrogate the fidelity of ABE. Analysis of *in silico* predicted off-target sequences (up to 4 mismatches) did not

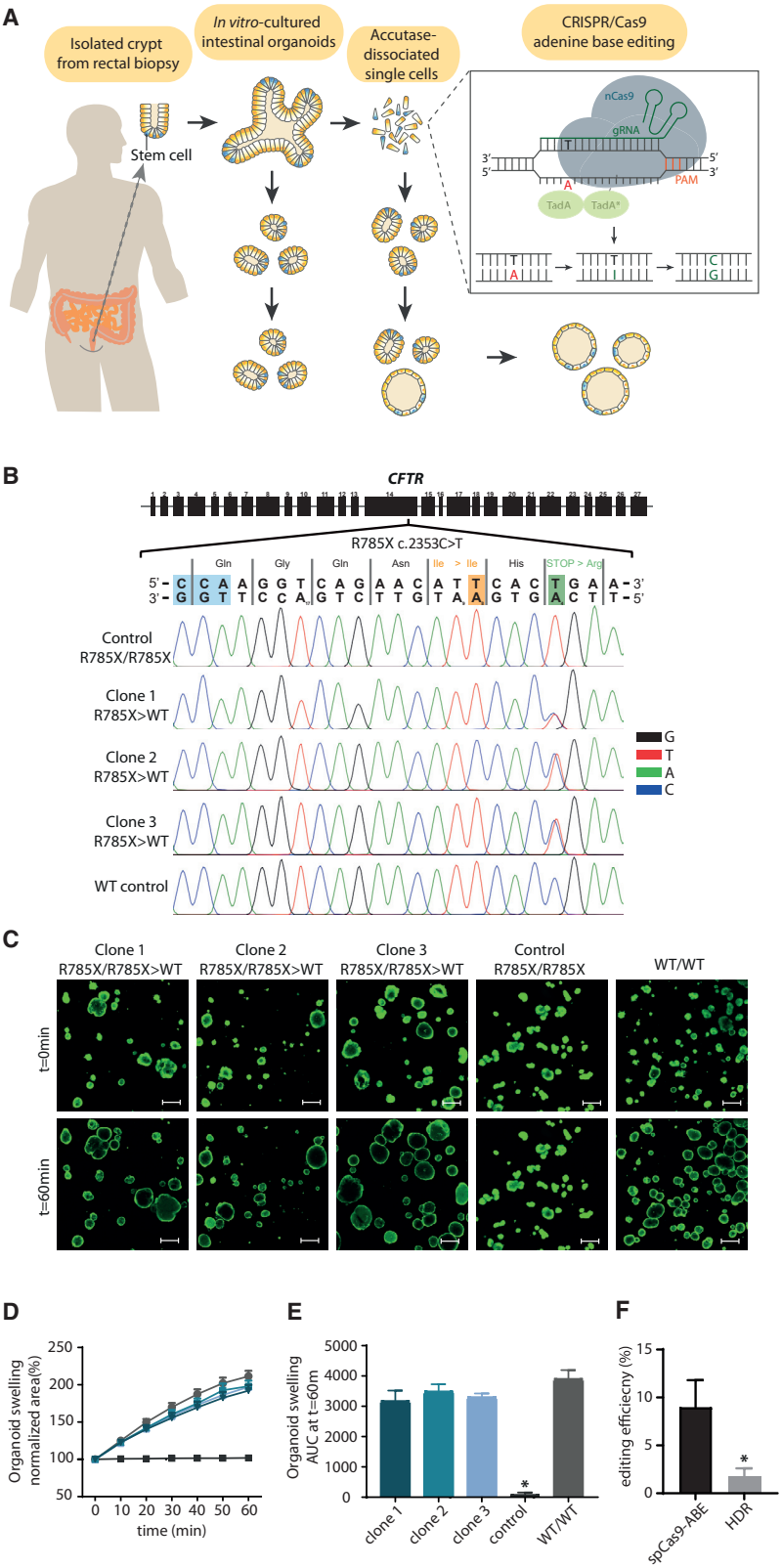

Figure 2. Adenine Base-Editing-Mediated Functional Repair of *CFTR* on Canonical PAM (NGG)

(A) Experimental design of ABE-mediated repair of *CFTR* in intestinal organoids.

(B) Sanger validation of R785X-*CFTR* repair using SpCas9-ABE in three clonal organoid cultures. The targeted base is highlighted in green, the off-target base is highlighted in orange, and the PAM is highlighted in blue.

(C) Confocal images of calcein-green-stained patient-derived intestinal organoids before and after 60 min. stimulation with forskolin (scale bars, 200 μm).

(D) Per well the total organoid area (xy plane in μm^2) increase relative to $t = 0$ (set to 100%) of forskolin treatment was quantified (n = 3).

(E) FIS as the absolute area under the curve (AUC) (t = 60 min; baseline, 100%), mean ± SD; n = 3, *p < 0.001, compared to the corrected organoid clones and the WT organoid sample.

(F) Editing efficiency quantified as fraction of FIS-assay-responsive organoids in the transfected pool. Bars represent mean ± SD; n = 5 and 3, *p < 0.05.

See also Figure S3.

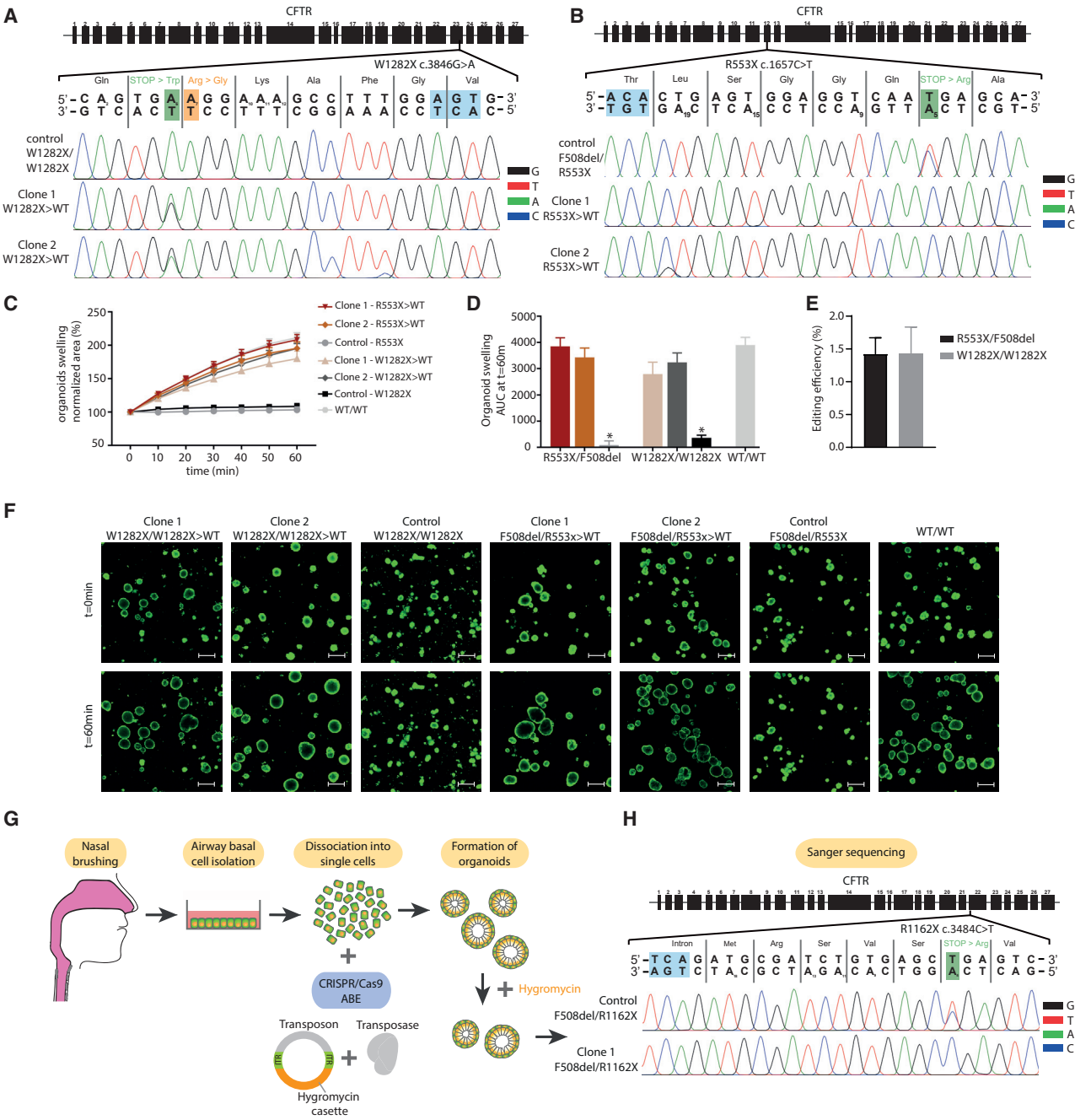

Figure 3. Adenine Base-Editing-Mediated Functional Repair of *CFTR* on Non-canonical PAMs (NGN)

(A) Sanger validation of R553X-*CFTR* repair in two corrected clonal lines.

(B) Sanger validation of W1282X-*CFTR* repair in two corrected clonal lines.

The targeted base in (A) and (B) is highlighted in green, the off-target base is highlighted in orange, and the PAM is highlighted in blue.

(C) Per well, the total organoid area (xy plane in μm^2) increase relative to t = 0 (set to 100%) of forskolin treatment was quantified.

(D) FIS as the absolute area under the curve (AUC) (t = 60 min; baseline, 100%), mean ± SD; n = 3 per CFTR mutation, *p < 0.001, compared to the corrected organoid clones and the WT organoid sample.

(E) Editing efficiency quantified as fraction of FIS-assay-responsive organoids in the transfected pool. Bars represent mean ± SD; n = 3 per CFTR mutation.

(F) Confocal images of calcein-green-stained patient-derived intestinal organoids before and after 60 min. stimulation with forskolin (scale bars, 200 μm).

(G and H) Experimental design of xCas9-ABE-mediated repair of R1162X-*CFTR* in airway organoids (G) and Sanger tracing of repaired and non-repaired airway organoids heterozygous for R1162X-*CFTR* (H).

See also Figure S3.

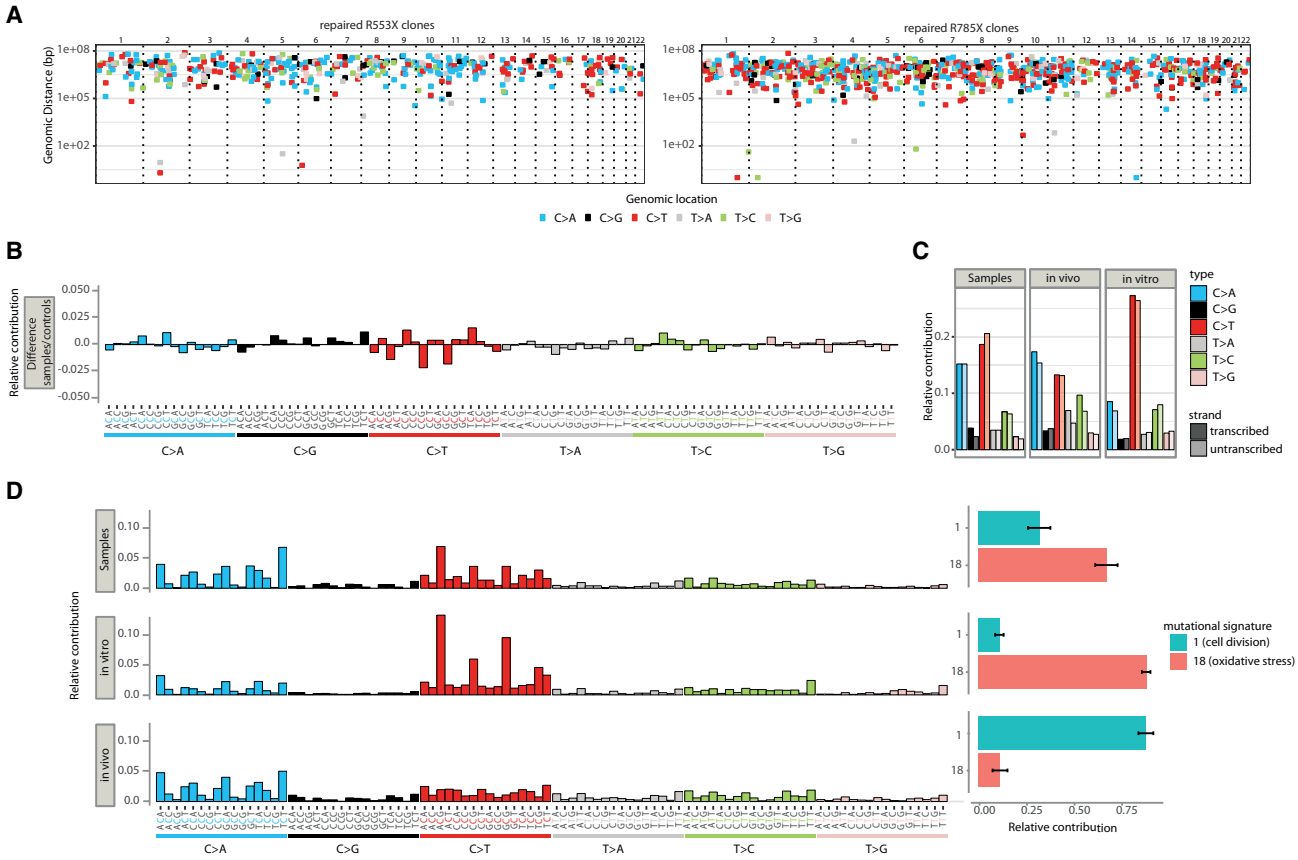

Figure 4. Off-Target Analysis of Adenine Base Editors

(A) Rainfall plots of repaired R553X and R785X clonal organoid lines. Every identified mutation is indicated with a dot (color according to mutation-type) and is ordered on the x axis from chromosome 1 to chromosome 22. The Y axis shows the distance between each mutation and the one prior to it (the genomic distance) and is plotted on a log scale.

(B) The mutational signature analysis, showed by the difference of the relative contribution of context-dependent mutation types between the repaired organoid lines (n = 6) and their respective unrepaired controls. The x axis shows al 96 context-dependent mutation types, a combination of the base substitution, and its neighboring bases. The y axis shows the relative contribution of each context-dependent mutation type.

(C) Relative contribution of mutations in our samples occurring on transcribed or un-transcribed regions in the genome compared to *in vitro* and *in vivo* acquired WGS datasets. The dark colored bars refer to the transcribed regions, while the light colored bars refer to the untranscribed regions.

(D) Mutational signature analysis of repaired organoid lines (n = 6) compared to an *in vitro* (n = 6) and *in vivo* (n = 6) dataset, and the relative contribution of the observed mutational signatures (1 and 18) in each dataset (bars represent mean ± SD).

reveal any off-target hits in the predicted off-target protospacer sequence or in the 100 flanking bases up- and downstream for both R785X (Table S3A) and R553X (Table S3B), in all repaired clones. Furthermore, no mutational hotspots (resulting from off-target sgRNA-dependent ABE binding) were observed in either of the samples on a genome-wide scale, as the rainfall plot (Figure 4A) does not present a region of hypermutation, shown by a cluster of dots at lower genomic distances. As the sample size in our study is small and differences in organoids culturing and propagation of individual clones are difficult to control for, we used a mutational signature analysis (Alexandrov et al., 2013a) to study base changes that could have been caused independent of cognate sgRNA binding. Signatures of repaired clones closely resembled those of the controls (cosine similarity of 0.92) and did not show an increase in T > C SNPs (the potential result of inadvertent, off-target ABE) (Figure 4B; Figure S4). We did not observe an increased number of mutations in highly transcribed regions, implying that the TadA fusion proteins did not cause mutations in single-stranded DNA segments, as may be present during transcription (Figure 4C). The main contributors to the total number of mutations in the corrected organoid lines were signature 1 and 18, previously described to be caused by *in vivo* generated cell-division-related mutations and *in vitro*-generated oxidative stress-related mutations, respectively (Alexandrov et al., 2013a). The mutational landscape of our SpCas9- and xCas9-ABE-repaired clones resulted from a combination of these two phenomena, as shown by a comparison to both *in vivo* (blood versus propagated clone) and *in vitro* (propagated clone versus subclone) WGS samples of the small and large intestine (Figure 4D). Finally, we confirmed the absence of known oncogenic mutation by comparison to a list of tumor suppressors and oncogenes extracted from COSMIC (Forbes et al., 2017), further supporting the safety of ABE (Tables S4A and S4B).

The current study demonstrates the feasibility of selective on-target base editing using ABE in human adult stem cells

derived from patients with an inherited disease. A large biobank capturing the broad diversity of CF mutations in the Dutch population was critical to this exploration. The biobank has been established for diagnostic purposes of rare CF cases and therefore—to some extent—overrepresents infrequent *CFTR* alleles. We have investigated the feasibility of performing ABE with two different versions of this technology. Our study demonstrates that xCas9-ABE (with a "relaxed" PAM sequence) can be applied effectively in human adult stem cells, emphasizing its clinical potential and applicability in the genetic repair of other inherited diseases. Functional repair of CFTR was obtained in rectal- and airway-derived organoids, while no genome-wide off-target effects could be detected, important for further development of ABEs. We have seen that editing efficiencies vary, depending on Cas9 and sgRNA usage, with a maximum of 9.3%. As it has been shown that 10% of residual CFTR function is associated with mild disease, this is within clinically relevant levels (Ferec and Cutting, 2012; Green et al., 2010). Furthermore, as we did not detect any genome-wide off-targets using either SpCas9-ABE or xCas9-ABE, multiple consecutive ABE treatments could be used to increase editing efficiencies of xCas9-ABE without any adverse off-target effects. It should be noted that to date, efficient *in vivo* delivery of the Cas9 genome editing apparatus in humans has been challenging. Taken together, our analyses extend observations on the fidelity of ABEs in rice (Jin et al., 2019) and mouse (Zuo et al., 2019) to the correction of disease-causing mutations in human stem cells.

STAR★METHODS

Detailed methods are provided in the online version of this paper and include the following:

- KEY RESOURCES TABLE
- LEAD CONTACT AND MATERIALS AVAILABILITY
- EXPERIMENTAL MODEL AND SUBJECT DETAILS
  - Biobank establishment and governance
- METHOD DETAILS
  - Intestinal organoid culture
  - Airway organoid culture
  - Plasmid construction
  - Intestinal organoid electroporation
  - Clonal expansion of intestinal organoids
  - Quantification of editing efficiency
  - Electroporation of basal progenitor cells
  - Clonal selection of airway organoids
  - Genotyping of clonal lines
  - FIS-assay
  - RNA extraction
  - Quantitative Real Time PCR
  - Western blotting
  - *In silico* target selection
  - Whole genome sequencing and mapping
  - Mutation calling and filtering
  - *In silico* off target prediction
  - Mutational signature analysis
- QUANTIFICATION AND STATISTICAL ANALYSIS
- DATA AND CODE AVAILABILITY

SUPPLEMENTAL INFORMATION

Supplemental Information can be found online at https://doi.org/10.1016/j.stem.2020.01.019.

ACKNOWLEDGMENTS

This work was supported by the NWO building blocks of life project: Cell dynamics within lung and intestinal organoids (737.016.009), CRUK Specificancer (C6307/A29058), and grants of the Dutch Cystic Fibrosis Foundation (NCFS), the Netherlands as part of the HIT-CF Program; the Dutch Health Organization ZonMw, the Netherlands. Furthermore, we would like to thank the FACS facility of the Princes Maxima Centre, Utrecht, the Netherlands, for allowing us to perform sorting and analysis experiments. S.Y.G. is a participant in the BIH-Charité Clinician Scientist Program funded by the Charité – Universitätsmedizin Berlin and the Berlin Institute of Health.

AUTHOR CONTRIBUTIONS

Conceptualization, M.H.G., E.d.P., J.M.B., and H.C.; Base-Editing Experiments, M.H.G. and E.d.P.; Writing – Original Draft, M.H.G. and E.d.P.; Writing – Review & Editing, M.H.G., E.d.P., J.M., H.M.J., K.M.d.W.-d.G., J.M.B., and H.C.; Supervision, J.M.B. and H.C.; Fluid Secretion & Biochemical Assays, M.H.G., E.d.P., and F.M.M.; Whole-Genome Sequencing Experiments and Analysis, M.H.G., E.d.P., R.O., and R.v.B.; Tissue Harvesting and Biobanking, P.v.M., G.B., K.M.d.W.-d.G., S.M., D.M., B.L.A., J.M., S.F.B., H.M.J., M.A.M., S.Y.G., and C.K.v.d.E.; Tissue Culturing, M.H.G., E.d.P., E.K., S.W.F.S., and J.E.B.; Funding Acquisition, J.M.B. and H.C.

DECLARATION OF INTERESTS

J.M.B. is an inventor on (a) patent(s) related to the FIS assay and received financial royalties from 2017 onward. J.M.B. reports receiving (a) research grant(s) and consultancy fees from various industries, including Vertex Pharmaceuticals, Proteostasis Therapeutics, Eloxx Pharmaceuticals, Teva Pharmaceutical Industries, and Galapagos outside the submitted work. H.C. holds several patents on organoid technology. Their application numbers, followed by their publication numbers (if applicable), are as follows: PCT/NL2008/050543, WO2009/022907; PCT/NL2010/000017, WO2010/090513; PCT/IB2011/002167, WO2012/014076; PCT/IB2012/052950, WO2012/168930; PCT/EP2015/060815, WO2015/173425; PCT/EP2015/077990, WO2016/083613; PCT/EP2015/077988, WO2016/083612; PCT/EP2017/054797, WO2017/149025; PCT/EP2017/065101, WO2017/220586; PCT/EP2018/086716, n/a; and GB1819224.5, n/a.

Received: July 2, 2019
Revised: December 11, 2019
Accepted: January 27, 2020
Published: February 20, 2020

REFERENCES

Alexandrov, L.B., Nik-Zainal, S., Wedge, D.C., Aparicio, S.A.J.R., Behjati, S., Biankin, A.V., Bignell, G.R., Bolli, N., Borg, A., Børresen-Dale, A.-L., et al.; Australian Pancreatic Cancer Genome Initiative; ICGC Breast Cancer Consortium; ICGC MMML-Seq Consortium; ICGC PedBrain (2013a). Signatures of mutational processes in human cancer. Nature *500*, 415–421.

Alexandrov, L.B., Nik-Zainal, S., Wedge, D.C., Campbell, P.J., and Stratton, M.R. (2013b). Deciphering signatures of mutational processes operative in human cancer. Cell Rep. *3*, 246–259.

Andersson-Rolf, A., Mustata, R.C., Merenda, A., Kim, J., Perera, S., Grego, T., Andrews, K., Tremble, K., Silva, J.C.R., Fink, J., et al. (2017). One-step generation of conditional and reversible gene knockouts. Nat. Methods *14*, 287–289.

Bae, S., Park, J., and Kim, J.S. (2014). Cas-OFFinder: a fast and versatile algorithm that searches for potential off-target sites of Cas9 RNA-guided endonucleases. Bioinformatics *30*, 1473–1475.

Berkers, G., van Mourik, P., Vonk, A.M., Kruisselbrink, E., Dekkers, J.F., de Winter-de Groot, K.M., Arets, H.G.M., Marck-van der Wilt, R.E.P., Dijkema,

J.S., Vanderschuren, M.M., et al. (2019). Rectal Organoids Enable Personalized Treatment of Cystic Fibrosis. Cell Rep. *26*, 1701–1708.e3.

Blokzijl, F., de Ligt, J., Jager, M., Sasselli, V., Roerink, S., Sasaki, N., Huch, M., Boymans, S., Kuijk, E., Prins, P., et al. (2016). Tissue-specific mutation accumulation in human adult stem cells during life. Nature *538*, 260–264.

Blokzijl, F., Janssen, R., van Boxtel, R., and Cuppen, E. (2018). MutationalPatterns: comprehensive genome-wide analysis of mutational processes. Genome Med. *10*, 33.

Boj, S.F., Vonk, A.M., Statia, M., Su, J., Vries, R.R., Beekman, J.M., and Clevers, H. (2017). Forskolin-induced Swelling in Intestinal Organoids: An In Vitro Assay for Assessing Drug Response in Cystic Fibrosis Patients. J. Vis. Exp. (120).

Cho, S.W., Kim, S., Kim, Y., Kweon, J., Kim, H.S., Bae, S., and Kim, J.S. (2014). Analysis of off-target effects of CRISPR/Cas-derived RNA-guided endonucleases and nickases. Genome Res. *24*, 132–141.

de Winter-de Groot, K.M., Janssens, H.M., van Uum, R.T., Dekkers, J.F., Berkers, G., Vonk, A., Kruisselbrink, E., Oppelaar, H., Vries, R., Clevers, H., et al. (2018). Stratifying infants with cystic fibrosis for disease severity using intestinal organoid swelling as a biomarker of CFTR function. Eur. Respir. J. *52*, 1702529.

Dekkers, J.F., Wiegerinck, C.L., de Jonge, H.R., Bronsveld, I., Janssens, H.M., de Winter-de Groot, K.M., Brandsma, A.M., de Jong, N.W.M., Bijvelds, M.J.C., Scholte, B.J., et al. (2013). A functional CFTR assay using primary cystic fibrosis intestinal organoids. Nat. Med. *19*, 939–945.

Dekkers, J.F., Berkers, G., Kruisselbrink, E., Vonk, A., de Jonge, H.R., Janssens, H.M., Bronsveld, I., van de Graaf, E.A., Nieuwenhuis, E.E.S., Houwen, R.H.J., et al. (2016). Characterizing responses to CFTR-modulating drugs using rectal organoids derived from subjects with cystic fibrosis. Sci. Transl. Med. *8*, 344ra84.

DePristo, M.A., Banks, E., Poplin, R., Garimella, K.V., Maguire, J.R., Hartl, C., Philippakis, A.A., del Angel, G., Rivas, M.A., Hanna, M., et al. (2011). A framework for variation discovery and genotyping using next-generation DNA sequencing data. Nat. Genet. *43*, 491–498.

Ferec, C., and Cutting, G.R. (2012). Assessing the Disease-Liability of Mutations in CFTR. Cold Spring Harb. Perspect. Med. *2*, 1–14.

Forbes, S.A., Beare, D., Boutselakis, H., Bamford, S., Bindal, N., Tate, J., Cole, C.G., Ward, S., Dawson, E., Ponting, L., et al. (2017). COSMIC: somatic cancer genetics at high-resolution. Nucleic Acids Res. *45* (D1), D777–D783.

Fu, Y., Foden, J.A., Khayter, C., Maeder, M.L., Reyon, D., Joung, J.K., and Sander, J.D. (2013). High-frequency off-target mutagenesis induced by CRISPR-Cas nucleases in human cells. Nat. Biotechnol. *31*, 822–826.

Fujii, M., Matano, M., Nanki, K., and Sato, T. (2015). Efficient genetic engineering of human intestinal organoids using electroporation. Nat. Protoc. *10*, 1474–1485.

Gaudelli, N.M., Komor, A.C., Rees, H.A., Packer, M.S., Badran, A.H., Bryson, D.I., and Liu, D.R. (2017). Programmable base editing of A·T to G·C in genomic DNA without DNA cleavage. Nature *551*, 464–471.

Green, D.M., McDougal, K.E., Blackman, S.M., Sosnay, P.R., Henderson, L.B., Naughton, K.M., Collaco, J.M., and Cutting, G.R. (2010). Mutations that permit residual CFTR function delay acquisition of multiple respiratory pathogens in CF patients. Respir. Res. *11*, 140.

Hu, J.H., Miller, S.M., Geurts, M.H., Tang, W., Chen, L., Sun, N., Zeina, C.M., Gao, X., Rees, H.A., Lin, Z., and Liu, D.R. (2018). Evolved Cas9 variants with broad PAM compatibility and high DNA specificity. Nature *556*, 57–63.

Jager, M., Blokzijl, F., Sasselli, V., Boymans, S., Janssen, R., Besselink, N., Clevers, H., van Boxtel, R., and Cuppen, E. (2018). Measuring mutation accumulation in single human adult stem cells by whole-genome sequencing of organoid cultures. Nat. Protoc. *13*, 59–78.

Jin, S., Zong, Y., Goa, Q., Zhu, Z., Wang, Y., Qin, P., Liang, C., Wang, D., Qia, J.-L., Zhang, F., et al. (2019). Cytosine, but not adenine, base editors induce genome-wide off-target mutations in rice. Science *8*, 647–656.

Jinek, M., Chylinski, K., Fonfara, I., Hauer, M., Doudna, J.A., and Charpentier, E. (2012). A programmable dual-RNA-guided DNA endonuclease in adaptive bacterial immunity. Science *337*, 816–821.

Keating, D., Marigowda, G., Burr, L., Daines, C., Mall, M.A., McKone, E.F., Ramsey, B.W., Rowe, S.M., Sass, L.A., Tullis, E., et al.; VX16-445-001 Study Group (2018). VX-445-Tezacaftor-Ivacaftor in Patients with Cystic Fibrosis and One or Two Phe508del Alleles. N. Engl. J. Med. *379*, 1612–1620.

Kleinstiver, B.P., Prew, M.S., Tsai, S.Q., Topkar, V., Nguyen, T., Zheng, Z., Gonzales, A.P.W., Li, Z., Randall, T., Yeh, J.J., et al. (2015). Engineered CRISPR-Cas9 nucleases with altered PAM specificities. Nature *523*, 481–485.

Koblan, L.W., Doman, J.L., Wilson, C., Levy, J.M., Tay, T., Newby, G.A., Maianti, J.P., Raguram, A., and Liu, D.R. (2018). Improving cytidine and adenine base editors by expression optimization and ancestral reconstruction. Nat. Biotechnol. *36*, 843–846.

Komor, A.C., Kim, Y.B., Packer, M.S., Zuris, J.A., and Liu, D.R. (2016). Programmable editing of a target base in genomic DNA without double-stranded DNA cleavage. Nature *533*, 420–424.

Kosicki, M., Tomberg, K., and Bradley, A. (2018). Repair of double-strand breaks induced by CRISPR-Cas9 leads to large deletions and complex rearrangements. Nat. Biotechnol. *36*, 765–771.

Li, H., and Durbin, R. (2010). Fast and accurate long-read alignment with Burrows-Wheeler transform. Bioinformatics *26*, 589–595.

Mali, P., Yang, L., Esvelt, K.M., Aach, J., Guell, M., DiCarlo, J.E., Norville, J.E., and Church, G.M. (2013). RNA-guided human genome engineering via Cas9. Science *339*, 823–826.

Mou, H., Vinarsky, V., Tata, P.R., Brazauskas, K., Choi, S.H., Crooke, A.K., Zhang, B., Solomon, G.M., Turner, B., Bihler, H., et al. (2016). Dual SMAD Signaling Inhibition Enables Long-Term Expansion of Diverse Epithelial Basal Cells. Cell Stem Cell *19*, 217–231.

Nishimasu, H., Shi, X., Ishiguro, S., Gao, L., Hirano, S., Okazaki, S., Noda, T., Abudayyeh, O.O., Gootenberg, J.S., Mori, H., et al. (2018). Engineered CRISPR-Cas9 nuclease with expanded targeting space. Science *361*, 1259–1262.

Pattanayak, V., Lin, S., Guilinger, J.P., Ma, E., Doudna, J.A., and Liu, D.R. (2013). High-throughput profiling of off-target DNA cleavage reveals RNA-programmed Cas9 nuclease specificity. Nat. Biotechnol. *31*, 839–843.

Ramsey, B.W., Davies, J., McElvaney, N.G., Tullis, E., Bell, S.C., Dřevínek, P., Griese, M., McKone, E.F., Wainwright, C.E., Konstan, M.W., et al.; VX08-770-102 Study Group (2011). A CFTR potentiator in patients with cystic fibrosis and the G551D mutation. N. Engl. J. Med. *365*, 1663–1672.

Rees, H.A., and Liu, D.R. (2018). Base editing: precision chemistry on the genome and transcriptome of living cells. Nat. Rev. Genet. *19*, 770–788.

Sachs, N., Papaspyropoulos, A., Zomer-van Ommen, D.D., Heo, I., Böttinger, L., Klay, D., Weeber, F., Huelsz-Prince, G., Iakobachvili, N., Amatngalim, G.D., et al. (2019). Long-term expanding human airway organoids for disease modeling. EMBO J. *38*, e100300.

Sato, T., Stange, D.E., Ferrante, M., Vries, R.G.J., Van Es, J.H., Van den Brink, S., Van Houdt, W.J., Pronk, A., Van Gorp, J., Siersema, P.D., and Clevers, H. (2011). Long-term expansion of epithelial organoids from human colon, adenoma, adenocarcinoma, and Barrett's epithelium. Gastroenterology *141*, 1762–1772.

Schwank, G., Koo, B.K., Sasselli, V., Dekkers, J.F., Heo, I., Demircan, T., Sasaki, N., Boymans, S., Cuppen, E., van der Ent, C.K., et al. (2013). Functional repair of CFTR by CRISPR/Cas9 in intestinal stem cell organoids of cystic fibrosis patients. Cell Stem Cell *13*, 653–658.

Sosnay, P.R., Siklosi, K.R., Van Goor, F., Kaniecki, K., Yu, H., Sharma, N., Ramalho, A.S., Amaral, M.D., Dorfman, R., Zielenski, J., et al. (2013). Defining the disease liability of variants in the cystic fibrosis transmembrane conductance regulator gene. Nat. Genet. *45*, 1160–1167.

Tarasov, A., Vilella, A.J., Cuppen, E., Nijman, I.J., and Prins, P. (2015). Sambamba: fast processing of NGS alignment formats. Bioinformatics *31*, 2032–2034.

Zafra, M.P., Schatoff, E.M., Katti, A., Foronda, M., Breinig, M., Schweitzer, A.Y., Simon, A., Han, T., Goswami, S., Montgomery, E., et al. (2018). Optimized base editors enable efficient editing in cells, organoids and mice. Nat. Biotechnol. *36*, 888–893.

Zhong, Z., Sretenovic, S., Ren, Q., Yang, L., Bao, Y., Qi, C., Yuan, M., He, Y., Liu, S., Liu, X., et al. (2019). Improving plant genome editing with high-fidelity xCas9 and non-canonical PAM-targeting Cas9-NG. Mol. Plant *12*, 1027–1036.

Zuo, E., Sun, Y., Wei, W., Yuan, T., Ying, W., Sun, H., Yuan, L., Steinmetz, L.M., Li, Y., and Yang, H. (2019). Cytosine base editor generates substantial off-target single-nucleotide variants in mouse embryos. Science *364*, 289–292.

STAR★METHODS

KEY RESOURCES TABLE

REAGENT or RESOURCE	SOURCE	IDENTIFIER
Antibodies		
Mouse anti-CFTR Immunoglobulins	Cystic Fibrosis Folding Consortium	450
Mouse anti-CFTR Immunoglobulins	Cystic Fibrosis Folding Consortium	570
Mouse anti-CFTR Immunoglobulins	Cystic Fibrosis Folding Consortium	596
Rabbit anti-HSP90 Immunoglobulins	Developed by laboratory of Prof. I. Braakman	N/A
Rabbit Anti-Mouse Immunoglobulins/HRP	Dako	P0260;RRID:AB_2636929
Goat Anti-Rabbit Immunoglobulins/HRP	Dako	P0448;RRID:AB_2617138
Bacterial Strain		
OneShot Mach1-T1 phage-resistante chemically competent *E.coli*	Thermofisher scientific	C862003
Biological Samples		
Human rectal tissue	This paper; http://hub4organoids.eu/	N/A
Human nasal tissue	This paper; University Medical Center Utrecht	N/A
Chemicals, Peptides, and Recombinant Proteins		
GlutaMax	Thermo Fisher Scientific: Invitrogen	#35050
HEPES	Thermo Fisher Scientific: Invitrogen	#15630-056
Wnt surrogate-Fc fusion protein	U-Protein Express	N001-0.5mg
Y-27632 Dihydrochloride (RhoKi)	Abmole bioscience	#Y-27632
Bronchial Epithelial Cell Growth Supplement (BEpiCGS)	Sciencell	#3262
Penicillin/Streptomycin	Thermo Fisher Scientific: Invitrogen	#15140-122
Primocin (50mg/ml)	InvivoGen	#ant-pm-1
Vancomycin	Sigma Aldrich	#861987- 250mg
Gentamycin	Life Technologies: GIBCO	#15710-049
Hygromycin B-gold 1 ml (100mg/ul)	InvivoGen	#ant-hg
BMPi (DMH-1)	Selleckchem	S7146
TGFb type I Receptor inhibitor (A83-01)	Tocris	#2939
B27 supplement	Thermo Fisher Scientific: Invitrogen	#17504-044
N-Acetylcysteine	Sigma Aldrich	#A9165
Nicotinamide	Sigma Aldrich	#N0636
p38 MAPK inhibitor (p38i) (SB202190)	Sigma Aldrich	#S7067
CHIR99021	Cayman Chemical	13122
FGF-7 Recombinant Human KGF	Peprotech	100-19_100ug
FGF10 Recombinant Human	Peprotech	100-26_1mg
Accutase	Thermofisher scientific	00-4555-56
TrypLE Express Enzyme	Thermo Fisher Scientific: Invitrogen	12605-028
Matrigel® (protein concentration > 10 mg/ml)	Corning	#356231
Q5 high fidelity polymerase	New England Biolabs	M0491
NEBbuilder Hifi Assembly mastermix	New England Biolabs	E2621
Dpn1	New England Biolabs	R0176
T4 DNA ligase	New England Biolabs	M0202
iQ™ SYBR Green Supermix	Bio-Rad	1708880
β-mercaptoethanol	Sigma Aldrich	#63700-50ml-F
Immobilon-FL Polyvinylidene difluoride (PVDF)-membrane	Merck Millipore	#IPFL00010

(*Continued on next page*)

Continued

REAGENT or RESOURCE	SOURCE	IDENTIFIER
cOmplete, Mini Protease Inhibitor Cocktail	Sigma Aldrich	11836153001
SuperSignal West Dura Extended Duration Substrate	Thermo Fisher	34075
ELK skimmed milk powder	Campina	N/A
BTXpress solution	BTX	MDS450805
Critical Commercial Assays		
Quick-DNA microprep kit	Zymogen	ZY-D3021
RNeasy mini kit	QIAGEN	74104
iScript™ cDNA Synthesis Kit	Bio-Rad	1708891
Pierce BCA Protein Assay Kit-1 L	Thermo Fisher Scientific	23225
DNeasy Blood & Tissue Kit	QIAGEN	69506
Deposited Data		
CFTR2 database	https://cftr2.org	N/A
Cystic Fibrosis Mutation Database	http://genet.sickkids.on.ca/	N/A
Dutch CF registry 2017	https://hub4organoids.eu/	N/A
Intestinal organoid biobank - Beekman laboratory governed	This paper	Table S1B
Intestinal organoid biobank - Hub Organoid Technology governed	This paper; https://hub4organoids.eu/	Table S1A
Single Nucleotide Polymorphism Database v137.b3730	https://www.ncbi.nlm.nih.gov/snp/	N/A
Index of mutational patterns in ASCs	Blokzijl et al., 2016; https://wgs11.op.umcutrecht.nl/mutational_patterns_ASCs/	N/A
Whole-genome sequencing data	https://ega-archive.org/	EGAS00001003951
Experimental Models: Cell Lines		
Human rectal organoid lines	This paper; http://hub4organoids.eu/	N/A
Airway organoid lines	This paper	N/A
Hek293T – Noggin hFc cell line	http://hub4organoids.eu/	N/A
Hek293T – R-spondin-1 mFc cell line	Trevigen Cat# 3710-001-K	N/A
Oligonucleotides		
Primers used for this manuscript	This paper	Methods S1
Recombinant DNA		
pCMV_ABEmax_P2A_GFP	Koblan et al., 2018	addgene#112101
pCMV_AncBE4max_P2A-GFP	Koblan et al., 2018	addgene#112100
pLenti-xFNLS-P2A-Puro	Zafra et al., 2018	addgene#110872
pMHG120_xABEmax_P2A_GFP	This paper	N/A
pMHG113_CMV_SpCas9_P2A_GFP	This paper	N/A
BPK1520	Kleinstiver et al., 2015	addgene#65777
pMHG031_CFTR_*785R	This paper	N/A
pMHG052_CFTR_*553R	This paper	N/A
pMHG099_CFTR_*1162R	This paper	N/A
pMHG100_CFTR_*1282W	This paper	N/A
Software and Algorithms		
Cellprofiler 3.1.5	https://cellprofiler.org/	N/A
Zen Image analysis software module	https://www.zeiss.com/microscopy/int/products/microscope-software/zen/image-analysis.html	N/A
SPSS	http://www.ibm.com//www.ibm.com/nl-en/products/spss-statistics	N/A
Graphpad prism	https://www.graphpad.com/scientific-software/prism/	N/A

(*Continued on next page*)

Continued

REAGENT or RESOURCE	SOURCE	IDENTIFIER
Adobe Illustrator	https://www.adobe.com/nl/products/illustrator.html	N/A
Ensembl BioMart (Ensembl Release 97)	https://www.ensembl.org/biomart/martview	N/A
Sambamba v0.4.7.32	Tarasov et al., 2015	N/A
GATK IndelRealigner v2.7.2	https://gatk.broadinstitute.org/hc/en-us	N/A
GATK BaseRecalibrator v2.7.2	https://gatk.broadinstitute.org/hc/en-us	N/A
GATK HaplotypeCaller v3.4-46	https://gatk.broadinstitute.org/hc/en-us; DePristo et al., 2011;	N/A
GATK-Queue v3.4-46	https://gatk.broadinstitute.org/hc/en-us	N/A
GATK VariantFiltration v3.4-46	https://gatk.broadinstitute.org/hc/en-us	N/A
Cas-OFFinder open recourse tool	Bae et al., 2014; http://www.rgenome.net/cas-offinder/	N/A
Burrows-Wheeler Aligner v0.5.9	Li and Durbin, 2010; http://bio-bwa.sourceforge.net/	N/A
Script for generation of somatic mutation catalogs	https://github.com/ToolsVanBox/SNVFI, https://github.com/ToolsVanBox/INDELFI; Blokzijl et al., 2016; Jager et al., 2018	N/A
Script for selection of ABE targets in CFTR2 database	https://github.com/MHgeurts/CRISPR-based-adenine-editors-correct-nonsense-mutations-in-a-cystic-fibrosis-organoid-biobank; Hu et al., 2018	N/A
Script for mapping of whole genome sequencing data	https://github.com/UMCUGenetics/IAP; Li and Durbin, 2010	N/A
R package for variant distribution visualization	This paper; Blokzijl et al., 2018; http://bioconductor.org/packages/release/bioc/html/MutationalPatterns.html	N/A
R package for extraction of mutational signatures	This paper; Blokzijl et al., 2018; http://bioconductor.org/packages/release/bioc/html/MutationalPatterns.html	N/A
R package for determining transcriptional strand bias	This paper; Blokzijl et al., 2018; http://bioconductor.org/packages/release/bioc/html/MutationalPatterns.html	N/A
R package for extracting and visualizing mutational patterns	https://github.com/CuppenResearch/MutationalPatterns/	N/A
Other		
Advanced Dulbecco's Modified Eagles Medium with Nutrient Mixture F-12 Hams (Ad-DF12) 500ml	Thermo Fisher Scientific: Invitrogen	#12634
Bronchial Epithelial Cell Medium (BEPICM)	Sciencell	#3211
R-spondin conditioned medium	Dekkers et al., 2013; Sato et al., 2011	N/A
Noggin conditioned medium	Dekkers et al., 2013; Sato et al., 2011	N/A
Intestinal organoid culture medium	Dekkers et al., 2016; Sato et al., 2011	N/A

LEAD CONTACT AND MATERIALS AVAILABILITY

Further information and requests for reagents may be directed to and will be fulfilled by the Lead Contact, H. Clevers (h.clevers@hubrecht.eu).

Genetically modified organoid lines generated in this study have been deposited to the UMCU biobank and are governed by Dr. J.M. Beekman in collaboration with the principle investigator that shipped the biopsy to UMCU.

EXPERIMENTAL MODEL AND SUBJECT DETAILS

No sample-size estimate was calculated before the study was executed. The experiments were not randomized. The investigators were not blinded to allocation during experiments and outcome assessment.

Biobank establishment and governance

All experimentation using human tissues described herein was approved by the medical ethical committee at University Medical Center Utrecht (UMCU; TcBio#14-008 and TcBio#16-586) and at Charite, Berlin. Informed consent for tissue collection (nasal and intestinal), generation, storage, and use of the organoids was obtained from all participating patients. Biobanked intestinal organoids (Table S1) are stored and cataloged (https://huborganoids.nl/) at the foundation Hubrecht Organoid Technology (http://hub4organoids.eu) and can be requested at info@hub4organoids.eu. Distribution of organoids to third parties (academic or commercial) requires completion of a material transfer agreement and will have to be authorized through a release protocol by the medical ethical committee at UMCU. These requests will be made by HUB in order to ensure compliance with the Dutch medical research involving human subjects' act. Use of organoids is subjected to patient consent; upon consent withdrawal, distributed organoid lines and any derived material will have to be promptly disposed of. Intestinal organoids from patients that did not gave broad informed consent for the HUB organoid technology (Table S2) were generated from intestinal biopsies which were obtained for (i) standard care, (ii) voluntary participation in scientific studies, or (iii) CF diagnostic questions in accordance with local ethical guidelines. In some cases, biopsies were directly sent from external hospitals to generate organoids without intestinal current measurements. The organoids are stored in the UMCU biobank and governed by Dr. J.M. Beekman in collaboration with the principle investigator that shipped the biopsy to UMCU. The use of these organoids for research is restricted to non-commercial research, and requires approval of the associated principal investigator who shipped the sample.

METHOD DETAILS

Intestinal organoid culture

Intestinal organoids stored in liquid nitrogen were thawed and passaged at least 4 times prior to electroporation. Furthermore, the mutations of the organoid lines used for the CRISPR/Cas9-ABE-experiments were first confirmed by Sanger sequencing. The culturing of the organoids was performed according to previously described protocols (Dekkers et al., 2016; Sato et al., 2011) except that the wnt-conditioned medium in the complete culture medium (CCM) was replaced by advanced DMEM-F12 supplemented with 1% HEPES, 1% Glutamax, 1% Pen/Strep (F12GHP), wnt-surrogate-Fc fusion protein (4 nM) and Y-27632 (10 μM) (CCM+). CCM+ was used as the standard culture medium in all intestinal organoid experiments unless stated otherwise.

Airway organoid culture

Nasal epithelial cells from a CF patient (F508del/R1162X) were collected from brushings of the inferior nasal turbinates using a cytological brush. Basal progenitor cells were isolated according to the dual SMAD inhibition method, previously described (Mou et al., 2016). In brief, brushed nasal cells were seeded in collagen type IV pre-coated tissue culture plates (Greiner) in BEPICM culture medium, supplemented with 1x BEpiCGS, Penicillin/Streptomycin (100 μg/ml), Primocin (50 μg/ml), Gentamicin (50 μg/ml), Vancomycin (100 μg/ml), Y-27632 (5 μM), DMH-1 (1 μM) and A83-01 (1 μM). After isolation and passaging for at least three times, the basal progenitor cells were electroporated (described in Method Details). Subsequent expansion of electroporated cells into organoids was performed in airway organoid medium (AO medium), adapted from Sachs et al. (2019), consisting of $F12^{GHP}$, Primocin (50 μg/ml), N-Acetylcysteine (1.25 mM), Nicotinamide (5 mM), 1x B27 supplement, P38 MAPK inhibitor (500 nM), Y-27632 (5 μM), A83-01 (1 μM), CHIR99021 (5 μM), 20% R-Spondin 1 conditioned medium (v/v), 20% Noggin conditioned medium (v/v), FGF7 (25 ng/ml), FGF10 (100 ng/ml).

Plasmid construction

Human codon optimized base editing constructs were a kind gift from David Liu; pCMV_ABEmax_P2A_GFP (Addgene plasmid#112101), pCMV_AncBE4max_P2A_GFP (Addgene plasmid#112100)(Koblan et al., 2018). Codon optimized xCas9 was a kind gift from Lukas Dow (pLenti-xFNLS-P2A-Puro, Addgene plasmid#110872)(Zafra et al., 2018). Q5 high fidelity polymerase was used to amplify the codon optimized xCas9 sequence and was cloned into the pCMV_ABEmax_P2A_GFP, using NEBbuilder HiFi assembly mastermix according to manufacturer protocols. Site-directed mutagenesis was performed to generate a D10A xCas9 nickase using T4 ligase and Dpn1 to religate the plasmid and to generate xCas9-ABE (pMHG120_xABEmax_P2A_GFP). The empty sgRNA plasmid backbone was a kind gift from Keith Joung (BPK1520, Addgene plasmid #65777). Spacer sequences targeting the different *CFTR* mutations were cloned in the sgRNA plasmid backbone using inverse PCR together with the same religation techniques as described above. All transformations in this study were performed using OneShot Mach1T1 cells and plasmid identity was checked by Sanger sequencing (Macrogen).

Intestinal organoid electroporation

The organoid electroporation protocol was adapted from Fujii et al. (2015). Organoids were maintained in CCM+ up until two days before electroporation. Two days in advance the Rspondin-conditioned medium in the CCM+ was replaced by $F12^{GHP.}$ One day in advance 1.25% (v/v) DMSO was added to the organoids. On the day of electroporation the organoids were dissociated into single cells using accutase supplemented with Y-27632 (10 μM) for 20 minutes and TrypLE supplemented with Y-27632 (10 μM) for 2 minutes, both at 37°C. In experiments based on FIS selection, the cell pellet (consisting of 10^6 cells) was resuspended in 90 μl BTXpress and combined with 10 μl plasmid solution (sgRNA-plasmid, 2.5 μg/μl, and pCMV_xABEmax_P2A_GFP-plasmid or pCMV_ABEmax_P2A_GFP-plasmid, 7.5 μg/μl). In the CRISPR/Cas9-mediated HDR experiments the plasmid solution contained

2.5 μg/μl sgRNA-plasmid, 7.5 μg/μl Cas9 expressing plasmid and 2.5μg/μl single stranded donor oligonucleotide containing a WT *CFTR* sequence and silent mutations to block Cas9 cleavage after repair. In experiments based on Hygromycin B-gold selection, the cell pellet was resuspended in 80 μl BTXpress and combined with 20 μl plasmid solution containing 2,5μg sgRNA-plasmid and 7,5μg pCMV_xABEmax_P2A_GFP-plasmid or pCMV_ABEmax_P2A_GFP-plasmid together with 10 μg PiggyBac transposon system (2.8 μg transposase + 7.2 μg hygromycin resistance containing transposon)) (Andersson-Rolf et al., 2017). Electroporation was performed using NEPA21 with settings described before (Fujii et al., 2015). After electroporation the cells were resuspended in 600ul matrigel (50% matrigel, 50% CCM+) and plated out in 20 μl droplet/well of a pre-warmed 48-wells tissue culture plates (Greiner). After polymerization, the matrigel droplets were immersed in 300 μL of CCM+ and the organoids were maintained at 37°C and 5% CO^2.

Clonal expansion of intestinal organoids

After an expansion period of at least 10 days the single cells grew out into organoids. Selection of genetically corrected organoids was based on CFTR function restoration and was assessed by adding forskolin (5 μM) to the CCM+. Pictures were made (1.25x with EVOS FL Auto Imaging System) prior to and 60 minutes after forskolin addition. Organoids that showed swelling after 60 minutes (indicating genetic restoration of *CFTR*) were individually picked with a p200 pipette and a bend p200 pipette tip. Each individual genetically corrected organoid was dissociated into single cells using accutase supplemented with Y-27632 (10 μM) for 5 minutes at 37°C. The cells were plated out in 20 μL matrigel droplets/picked organoid (50% matrigel, 50% CCM+) in pre-warm 48-well tissue culture plates (Greiner) and maintained at 37°C and 5% CO^2. The single cells were grown toward clearly separated, single organoid structures and corrected organoids were picked and passaged after visual screening of FIS until a clonal organoid culture was established. This was confirmed by Sanger sequencing and the absence of FIS-assay unresponsive organoids after repeated passaging.

Quantification of editing efficiency

Two days after electroporation of the intestinal organoids harboring the R785X mutation, we first selected the transfected cells by FACS sorting based on GFP, expressed by the pCMV_xABEmax_P2A_GFP-plasmid or pCMV_ABEmax_P2A_GFP-plasmid on a Moflo Astrios (Beckman Coulter). The GFP+ cells were plated out (500 cells/20 μl matrigel ((50% matrigel, 50% CCM+) droplet) in pre-warm 48-wells plates and expanded for 7-9 days. To determine the editing efficiency in the pool of transfected R785X/R785X organoids, the total number of organoids was quantified using Cellprofiler 3.1.5. Next, the number of corrected organoids were identified by counting the FIS-assay responsive organoids. For the organoid lines harboring W1282X/W1282X and R553X/F508del mutations, two days post transfection, we took 20% of the electroporated cells and determined the transfection efficiency by FACS analysis on a Moflo Astrios (Beckman Coulter) as described above. The remainder of transfected non-sorted organoids were then diluted and plated (250 organoids/20 μl matrigel ((50% matrigel, 50% CCM+) droplet) pre-warm 48-wells plates and expanded for 7-9 days. We then quantified the total amount of cultured organoids by using cell-profiler 3.1.5. Editing efficiencies were determined by dividing the total amount of organoids by the transfection efficiency and the amount of FIS-assay responsive organoids.

Electroporation of basal progenitor cells

After expansion (at least passage three) of the basal progenitor cells (2D-monolayer) in collagen type IV pre-coated tissue culture plates they were dissociated with TrypLE for 10 minutes at 37°C @. The single basal progenitor cells were electroporated according to the protocol described in the section 'intestinal organoid electroporation'. Next, cells were seeded in a density of $9x10^4$ cells per 30 μl matrigel (75% matrigel, 25% AO medium) droplets in a pre-warmed 24 wells suspension plates (Greiner). After solidification, droplets were overlaid with 500 μL airway AO medium and the organoids were maintained at 37°C and 5% CO2.

Clonal selection of airway organoids

The electroporated cells grew out into organoids and after three days hygromycin (1:1000) was added to the AO culture medium to select for transfected organoids. After 4-7 days the organoids were passaged and hygromycin treatment was continued until all control organoids (not electroporated with PiggyBac-plasmids) were killed. The hygromycin resistant clones were individually picked and passaged using the same protocol as for the corrected intestinal organoids. The organoid-derived single cells were plated out in 30 μl matrigel/well of a 24-well suspension plate (75% matrigel, 25% AO medium) and were overlaid with 500 μl AO medium and maintained at 37°C and 5% CO2. DNA of each individual organoid clone was harvested and gene correction was assessed with Sanger sequencing.

Genotyping of clonal lines

Intestinal and airway organoid DNA was harvested from 10-20μL Matrigel/organoid suspension and DNA was extracted using the Quick-DNA microprep kit. Target regions were amplified from the genome using Q5 high fidelity polymerase primers for target region amplification can be found in Methods S1. Sequencing was performed using the M13F tail as all forward amplification primers for targeted sequencing contained a tail with this sequence. Base editing induced genomic alterations were confirmed by Sanger sequencing (Macrogen).

FIS-assay

To quantify the CFTR function restoration in the genetically corrected intestinal clones the FIS-assay was conducted in duplicate at three independent culture time points (n = 3) according to previous published protocols (Boj et al., 2017; Dekkers et al., 2016). In short, intestinal organoids were seeded in 96-well culture plates (Nunc) in 4 μL of 50% matrigel (+50% CCM+) containing 20 to 40 organoids and immersed in 50 μL CCM+. The day after, organoids were incubated for 30 min with 3 μM calcein green (Invitrogen) to fluorescently label the organoids and stimulated with 5 μM forskolin. Every ten minutes the total calcein green labeled area per well was monitored by a Zeiss LSM800 confocal microscope, for 60 minutes while the environment was maintained at 37°C and 5% CO2. A Zen Image analysis software module (Zeiss) was used to quantify the organoid response (area under the curve measurements of relative size increase of organoids after 60 minutes forskolin stimulation, t = 0 min baseline of 100%).

RNA extraction

RNA was isolated with the RNeasy Mini kit (QIAGEN) with a DNase digestion step (RNase-Free DNase Set, QIAGEN) according to manufacturer's instructions. In short, the intestinal organoids were harvested at three independent culture time points (n = 3) in $F12^{GHP}$ and mechanically disrupted according to previous described protocol (Berkers et al., 2019; Dekkers et al., 2016; Sato et al., 2011). After spinning down, the supernatant was removed and the pellet was resuspended in 350 mL RLT buffer (RNeasy Mini kit QIAGEN) + β-mercaptoethanol (1%) by a 1 minute vortex. The lysates were immediately used or stored at −80°C. The amount and purity of the RNA samples was determined with the Nanodrop ND-1000 spectrophotometer (Thermo Scientific). CDNA ranging from 500 ng to 1 μg RNA was obtained with the iScript™ cDNA Synthesis Kit (BIO-RAD) using the supplier's protocol.

Quantitative Real Time PCR

10 μL qRT-PCR reactions were performed using BIO-RAD I-Cycler 96 wells-plates, iQ™ SYBR Green Supermix (BIO-RAD), 0.4 μM forward primer and 0.4 μM reverse primer. The samples, harvested at three different culture time points (n = 3), were analyzed in triplicate using a two-step real time quantitative PCR (BIO-RAD). For each primer the annealing temperature resulting in 95%–105% amplifying efficiency was determined with a gradient PCR. The amount of mRNA per sample was determined using the Livak method, (CT values were normalized with mean mRNA expression of the housekeeping genes YWAZ and β-ACTIN). Primers used for qPCR are listed in Methods S1.

Western blotting

First intestinal organoids were harvested in $F12^{GHP}$, washed with PBS and mechanically disrupted at three different culture time points (n = 3). After spinning down the pellets were lysed with Laemmli buffer (4% SDS, 20% glycerol, 12% 1M Tris (pH 6.8) in MQ) supplemented with a complete protease inhibitor tablet (1 tablet/50 ml) and stored at −80°C. After thawing, the lysate suspension was homogenized and protein concentration was determined in duplicate with the BCA protein assay according to manufacturer's protocol. 50 mg protein was loaded per 50ul slots in a 6% agarose gel. The proteins were separated with SDS-page and transferred to Immobilon-FL Polyvinylidene difluoride (PVDF)-membrane using wet tank transfer O/N at 4°C. The membranes were blocked for 1 hour with Tris-buffered Saline Tween (TBST) containing 5% milk protein (ELK Campina). The membranes were incubated with TBST containing 0.5% milk protein and a pool of anti-CFTR mouse antibodies (Cystic Fibrosis Folding Consortium 450, 570 and 596; diluted 1:15000) and anti-HSP90 (diluted 1:50.000) rabbit antibodies for 3 hours at 4°C. The membranes were cut at 100 KDa and incubated with goat-anti-mouse (diluted 1:5000) or goat-anti-rabbit (diluted 1:2000) horseradish peroxidase-conjugated secondary antibody in TBST containing 0.5% milk protein. Three 15-minute wash steps with TBST and one 10-minute wash step with PBS were conducted. The PVDF membranes (one membrane per harvesting time point, n = 3) were incubated for 5 minutes with SuperSignal West Dura Extended Duration Substrate and were developed with the ChemiDoc Touch Imaging System (BIO-RAD).

In silico target selection

To select potential CBE and ABE targets from the CFTR2 database we adapted the target calling script from Hu et al. (2018). Ensembl BioMart (Ensembl Release 97) was used to extract flanking sequences of all CFTR2 described SNPs. The used pipeline can be found on: https://github.com/MHgeurts/CRISPR-based-adenine-editors-correct-nonsense-mutations-in-a-cystic-fibrosis-organoidbiobank.

Whole genome sequencing and mapping

Genomic DNA was isolated from 100 μl of Matrigel/organoid suspension using DNeasy Blood & Tissue Kit, according to protocol. Standard Illumina protocols were applied to generate DNA libraries for Illumina sequencing from 20-50ng of genomic DNA. All samples (three genetically corrected clones and one non-corrected control sample of the R785X/R785X and R553X/F508del donor) were sequenced (2x150bp) by using Illumina NovaSeq to 30x base coverage. Reads were mapped against human reference genome hg19 using Burrows-Wheeler Aligner v0.5.9(Li and Durbin, 2010), with settings 'bwa mem -c 100 -M'. Duplicate sequence reads were marked using Sambamba v0.4.7.32 and realigned per donor using Genome Analysis Toolkit (GATK) IndelRealigner v2.7.2 and quality scores were recalibrated using the GATK BaseRecalibrator v2.7.2. More details on the pipeline can be found on https://github.com/UMCUGenetics/IAP.

Mutation calling and filtering

Raw variants were multisample-called by using the GATK HaplotypeCaller v3.4-46(DePristo et al., 2011) and GATK-Queue v3.4-46 with default settings and additional option 'EMIT_ALL_CONFIDENT_SITES'. The quality of variant and reference positions was evaluated by using GATK VariantFiltration v3.4-46 with options '-snpFilterName LowQualityDepth -snpFilterExpression "QD < 2.0" -snpFilterName MappingQuality -snpFilterExpression "MQ < 40.0" -snpFilterName StrandBias -snpFilterExpression "FS > 60.0" -snpFilterName HaplotypeScoreHigh -snpFilterExpression "HaplotypeScore > 13.0" -snpFilterName MQRankSumLow -snpFilterExpression "MQRankSum < −12.5" -snpFilterName ReadPosRankSumLow -snpFilterExpression "ReadPosRankSum < −8.0" -cluster 3 -window 35'. To obtain high-quality somatic mutation catalogs, we applied post processing filters as described (Blokzijl et al., 2016). Briefly, we considered variants at autosomal chromosomes without any evidence from a paired control sample (MSCs isolated from the same bone marrow); passed by VariantFiltration with a GATK phred-scaled quality score $\geq$ 250; a base coverage of at least 20X in the clonal and paired control sample; no overlap with single nucleotide polymorphisms (SNPs) in the Single Nucleotide Polymorphism Database v137.b3730; and absence of the variant in a panel of unmatched normal human genomes (BED-file available upon request). We additionally filtered base substitutions with a GATK genotype score (GQ) lower than 99 or 10 in the clonal or paired control sample, respectively. For indels, we filtered variants with a GQ score lower than 99 in both the clonal and paired control sample and filtered indels that were present within 100 bp of a called variant in the control sample. In addition, for both SNVs and INDELs, we only considered variants with a mapping quality (MQ) score of 60 and with a variant allele frequency of 0.3 or higher in the clones to exclude *in vitro* accumulated mutations (Blokzijl et al., 2016; Jager et al., 2018). The scripts used are available on GitHub (https://github.com/ToolsVanBox/SNVFI, https://github.com/ToolsVanBox/INDELFI). The distribution of variants was visualized using an in house developed R package (MutationalPatterns) (Blokzijl et al., 2018).

In silico off target prediction

Potential sgRNA specific off-target events were predicted using the Cas-OFFinder open recourse tool (Bae et al., 2014). All potential off-targets up to 4 mismatches were taken into account. For *CFTR*-R785X an NGG PAM and for *CFTR*-R553X an NGN PAM was selected.

Mutational signature analysis

We extracted mutational signatures and estimated their contribution to the overall mutational profile as described (Alexandrov et al., 2013b) using an in house developed R package (MutationalPatterns) (Blokzijl et al., 2018) **(**Methods S2**)**. In this analysis, we included small intestine data (previously analyzed) to explicitly extract *in vivo* and *in vitro* accumulated signatures (Blokzijl et al., 2016). To determine the transcriptional strand contribution and bias, we selected all point mutations that fall within gene bodies and checked whether the mutated base was located on the transcribed or non-transcribed strand. We used a in house developed R package (MutationalPatterns) to determine transcriptional strand bias as described (Blokzijl et al., 2018).

QUANTIFICATION AND STATISTICAL ANALYSIS

Statistical parameters are reported in the figure legends and the 'Method Details' section. The mean forskolin-induced swelling (AUC) and ΔCT of non-corrected control clone was compared to the mean forskolin-induced swelling and ΔCT of genetically corrected organoid clones. First the Levene's test was conducted and a QQ-plot of the residuals of the AUC and ΔCT values was made, which proved homogeneity of variances and normal distribution of the residuals. Subsequently, the One-way ANOVA was used to assess whether the differences in mean swelling and mean ΔCT between the groups were statistically significant (α > 0,05). To assess whether the AUC and ΔCT of the individual clones were significantly different from the non-corrected controls the Dunnet's test was conducted. To assess whether the difference in mean editing efficiencies between the SpCas9-ABE and HDR-treated organoids is statistically significant (α > 0,05) a paired t test was performed after homogeneity of variances (Levene's test) and normality of the error distribution (QQ-plot of the residuals) was confirmed.

DATA AND CODE AVAILABILITY

All software tools can be found online (see Key Resources Table). The accession number for the whole-genome sequencing datasets reported in this paper is European Genome-Phenome Archive:EGAS00001003951.

Cell Stem Cell, Volume *26*

Supplemental Information

CRISPR-Based Adenine Editors Correct Nonsense Mutations in a Cystic Fibrosis Organoid Biobank

Maarten H. Geurts, Eyleen de Poel, Gimano D. Amatngalim, Rurika Oka, Fleur M. Meijers, Evelien Kruisselbrink, Peter van Mourik, Gitte Berkers, Karin M. de Winter-de Groot, Sabine Michel, Danya Muilwijk, Bente L. Aalbers, Jasper Mullenders, Sylvia F. Boj, Sylvia W.F. Suen, Jesse E. Brunsveld, Hettie M. Janssens, Marcus A. Mall, Simon Y. Graeber, Ruben van Boxtel, Cornelis K. van der Ent, Jeffrey M. Beekman, and Hans Clevers

Supplemental Items

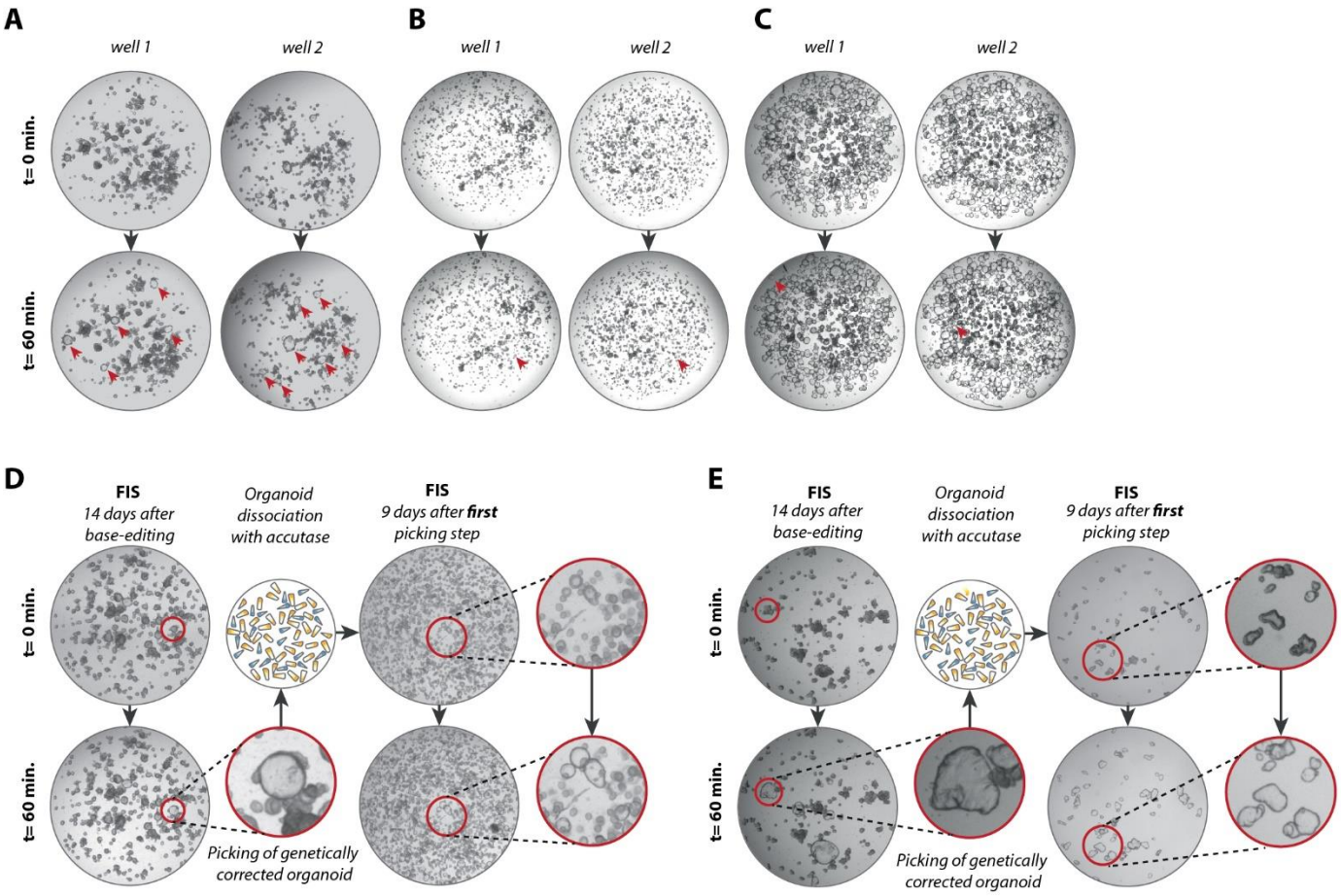

Supplementary Figure 1: Phenotypic selection and clonal expansion of ABE-repaired organoids, related to Figure 2 and 3.

Bright field images before and after 60 min forskolin stimulation of bulk organoid cultures after electroporation, harboring R785X/R785X **(A)**, F508del/R553X **(B)**, and W1282X/W1282X-CFTR mutations **(C)**. Organoids responding to forskolin (highlighted by the red arrowheads) were visually selected **(D)**, picked and expanded until a clonal organoid culture was established. **(E)** Picking and passaging of one individual FIS-assay responsive organoid upon FACS sorting of GFP-positive cells results in a clonal organoid culture where all organoids are FIS-assay responsive. This shows that the original organoid exclusively consists of repaired cells.

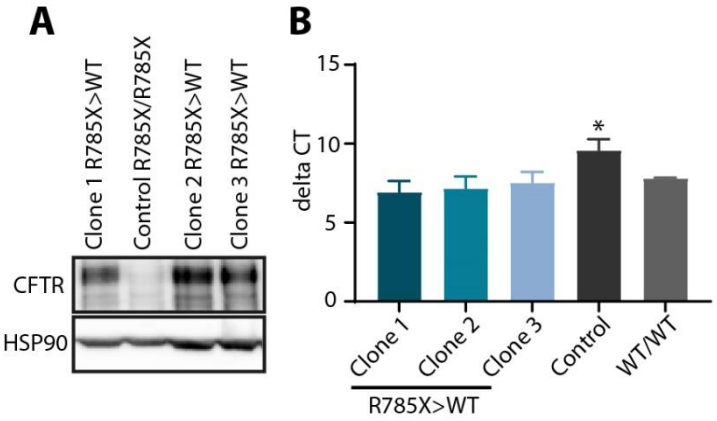

Supplementary Figure 2: protein and mRNA expression of SpCas9-ABE-corrected organoids, related to Figure 2.

(A) Western-blot analysis of R785X-CFTR repair using SpCas9-ABE in three corrected clonal organoid cultures compared to non-corrected control R785X/R785X organoids. **(B)** qPCR deltaCT values of the same repaired clonal organoid cultures compared to non-corrected control organoids, bars represent mean ±SD; *N*=4.

A

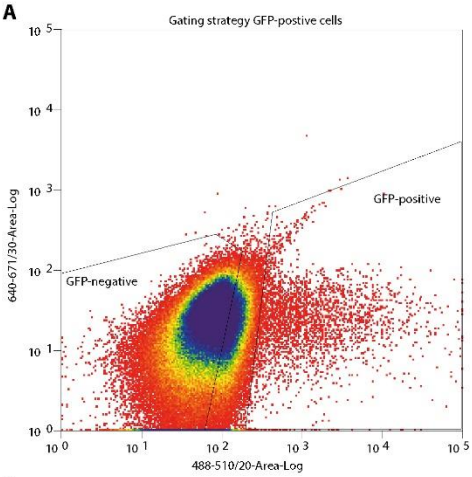

B

Sample name	# organoid outgrowth	Transfection efficiency	Amount of transfected organoids	Amount of repaired organoids	Editing efficiency	Mean editing efficiency
SpABE-785/785 n=1	*	1.71%	220	20	9.09%	8.98%
SpABE-785/785 n=2	*	0.51%	30	4	13.33%	
SpABE-785/785 n=3	*	1.55%	267	20	7.49%	
SpABE-785/785 n=4	*	1.7%	432	40	9.26%	
SpABE-785/785 n=5	*	1.99%	385	22	5.71%	
HDR-785/785 n=1	*	4.28%	689	6	0.87%	1,78%
HDR-785/785 n=2	*	3.12%	704	14	1.98%	
HDR-785/785 n=3	*	3.11%	765	19	2.48%	
xABE - 1282/1282 n=1	17689	5.9%	1044	15	1.44%	1.43%
xABE - 1282/1282 n=2	16652	4.33%	721	12	1.66%	
xABE - 1282/1282 n=3	14819	4.59%	680	8	1.18%	
xABE - 553/F508del n=1	34634	3.29%	1140	19	1.67%	1.43%
xABE - 553/F508del n=2	37407	2.25%	842	14	1.66%	
xABE - 553/F508del n=3	42221	2.19%	925	9	0.97%	

*Organoids sorted

Supplementary Figure 3: editing efficiensies in intestinal organoids, related to Figure 2 and 3.

GFP-postive cells were either sorted (* in **B**) or quantified using the gating strategy depicted in **(A)**. The editing efficiencies were calculated by dividing the total number of organoids with the transfection efficiency (only for the samples that were not sorted) and the total number of organoids that showed a swelling response upon 1h stimulation with forskolin **(B)**.

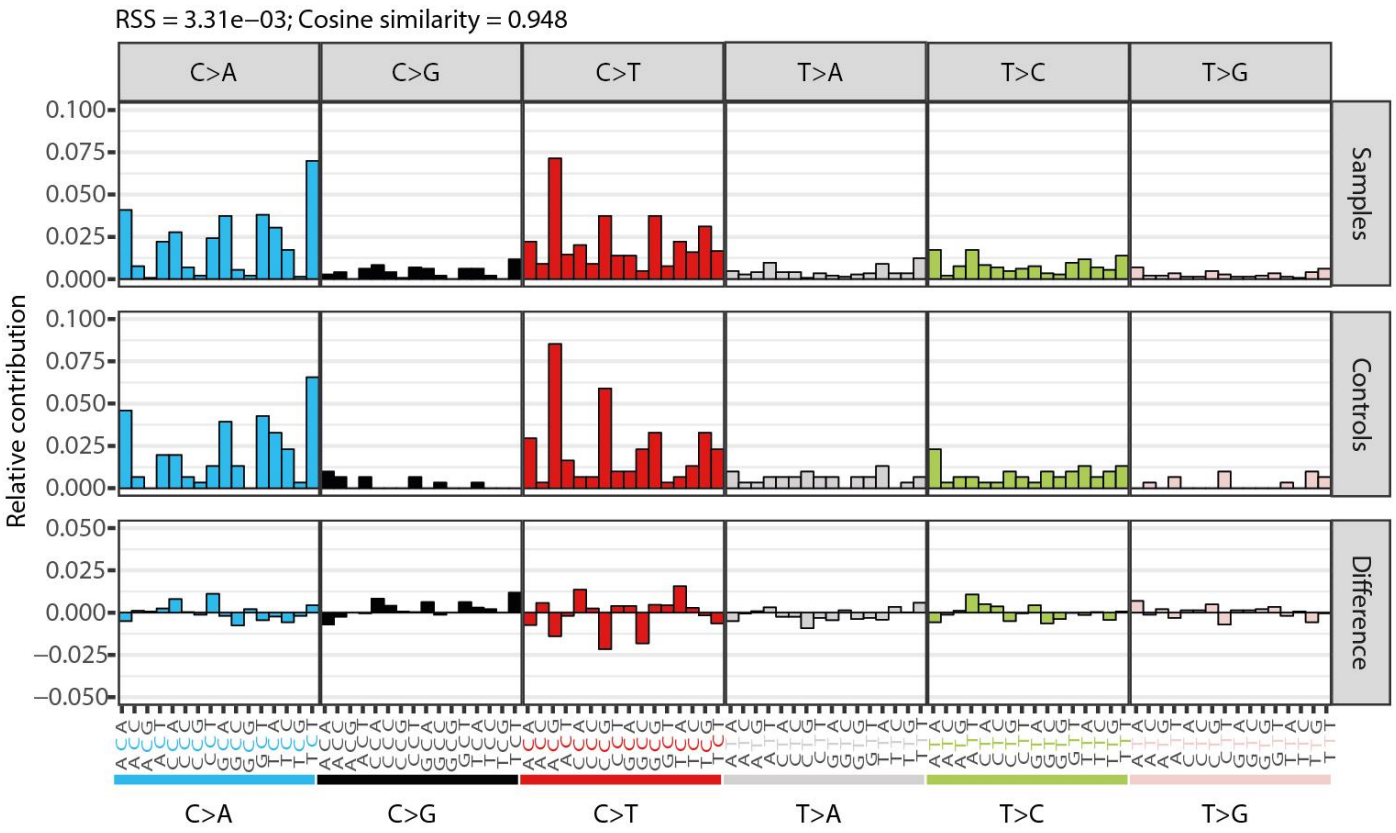

Supplementary Figure 4: mutational signature and strand bias analysis on WGS data, related to Figure 4.

Relative contribution of mutations in three repaired R785X/R785X clonal organoid lines and three R553X/F508del clonal organoid lines. The X-axis shows al 96 context-dependent mutation types, which is a combination of the base substitution and its neighbouring bases. The Y-axis shows the relative contribution of each mutation type.